2012

The ethanol electrooxidation at Pt layers deposited on polycrystalline Au

PHYSICAL CHEMISTRY CHEMICAL PHYSICS, CAMBRIDGE, v. 14, n. 2, pp. 599-606, MAY, 2012
http://www.producao.usp.br/handle/BDPI/33443

PCCP

Cite this: *Phys. Chem. Chem. Phys.*, 2012, **14**, 599–606

www.rsc.org/pccp

PAPER

The ethanol electrooxidation at Pt layers deposited on polycrystalline Au

Mauricio J. Prieto,*[a] Ubirajara P. Rodrigues Filho,[a] Richard Landers[b] and Germano Tremiliosi-Filho[a]

Received 22nd July 2011, Accepted 24th October 2011
DOI: 10.1039/c1cp22390a

The ethanol electro-oxidation reaction was evaluated using a polycrystalline Au substrate modified with two different amounts of Pt using the galvanic exchange methodology. FTIR results suggest that Pt deposits have a greater ability to break the C–C bond present in the ethanol molecule. However, under potentiostatic conditions both modified Au surfaces undergo faster deactivation in comparison with polycrystalline platinum as indicated by the chronoamperometric results. XPS results indicate the presence of two phases depending on the Pt content. These are: (i) Pt–Au alloy and (ii) segregated Pt. The structural and electronic properties of these phases were related to the differences observed in the catalytic activity.

Introduction

Over the last 20 years much effort has been made in order to develop the technology necessary to ensure an efficient use of energy sources and a special attention was given to the renewable ones. One of the fields of great interest which promises to minimize the environmental problems with fossil fuels is the Fuel Cells area. In all their variants (SOFCs, MCFCs, DAFCs), fuel cells are intended to be a clean energy source, using the chemical energy contained in the fuel molecules to provide electricity that might be used in a wide variety of areas, such as automobile applications, portable devices (telephones, PDAs, Laptops), spacecraft programs, *etc*.

Among all types of fuel cells, the Direct Alcohol Fuel Cells have called the attention of researchers all over the world in the last few years, due to the possibility of using alcohols obtained from the fermentation of different sources of biomass, such as ethanol (*e.g.* from sugar fermentation).

Moreover, when ethanol is compared with methanol as a fuel candidate, the former has some advantages due to its low toxicity and the higher electron efficiency that could be achieved if the C–C bond breaking route is followed. Unfortunately, direct ethanol fuel cells (DEFCs) are still presenting power densities and efficiencies below the required level for commercialization. This is, basically, because of the complexity of the oxidation reaction network and the high energy barrier for C–C bond breaking, a reaction step that is important for achieving the maximum number of electrons per alcohol molecule (12). On the other hand, the low availability of Pt makes it impossible to envisage a wide scale application of fuel cells containing high Pt-based catalyst loadings. Hence, catalysts with ultra-low Pt content may offer a solution to this problem. These low Pt content catalysts have already been tested by several groups for oxygen reduction reaction,[1–3] methanol[4–7] and formic acid[8] oxidation. Nevertheless, there are a few studies in the literature on the electro-oxidation of ethanol over these kinds of catalysts (see *e.g.* ref. 9).

In order to provide some insights into the electro-oxidation mechanism of ethanol and the stability of Pt shells, we propose the use of modified polycrystalline Au surfaces as model substrates which might allow the understanding of the behavior of core–shell nanoparticles. In the present paper we show the results obtained in such study with the aim to provide some insights into the reaction and its dependence on Pt coverage.

Experimental section

The working electrode used was a 6 mm diameter gold cylinder (99.999% Mateck) press-fitted in a Teflon holder. It was polished, starting with an emery paper followed by alumina suspensions from 9.0 down to 0.05 μm on microcloth pads until a mirror like surface was obtained. After the polishing procedure, the working electrode was left in an ultrasound bath for 1 h to remove alumina residues.

All electrochemical experiments were performed in a three electrode compartment glass cell. A hydrogen electrode prepared in the acidic electrolyte solution was used as the reference electrode and a gold foil as a counter electrode. Before each measurement, the working electrode was left in contact with a H_2SO_4 : H_2O_2 mixture for 5 min, rinsed with fresh Milli-Q water and immediately admitted in the electrochemical cell to avoid further contamination. A *Solartron 1285 potentiostat* was used to perform all electrochemical experiments. All solutions used in experiments were prepared from Milli-Q water and high purity reagents. The surface cleanliness of the working electrode

[a] *Instituto de Química de São Carlos, Universidade de São Paulo, C.P. 780, 13566.970, São Carlos, SP, Brazil. E-mail: prietomauricio@gmail.com*
[b] *Instituto de Física Gleb Wataghin, Unicamp, C.P. 6165, 13083-970, Campinas, SP, Brazil*

was checked using cyclic voltammetry and before Pt deposition, the gold surface was cycled in a 0.1 mol L^{-1} $HClO_4$ solution. All voltammograms were recorded using a 50 mV s^{-1} sweep rate.

In order to obtain the Pt deposits by galvanic exchange, a Cu monolayer was previously deposited on the Au surface from a 0.05 mol L^{-1} $CuSO_4$ + 0.1 mol L^{-1} $HClO_4$ electrolytic solution. Once the Cu monolayer was deposited, the Cu modified surface was introduced in oxygen free 0.2 mmol L^{-1} K_2PtCl_4 or H_2PtCl_6 solution, in order to obtain the ideal Pt monolayer or half monolayer, respectively.

Pt deposits stability was investigated using cyclic voltammetry in a 0.1 mol L^{-1} $HClO_4$ solution. To do so, the Pt modified surface was cycled within different anodic potential cuts and then, the 10th cycles of each potential excursion were compared in order to detect possible differences in the voltammetric profiles.

With the aim of investigating the ethanol electro-oxidation reaction over the Pt modified Au surfaces, voltammetric and chronoamperometric experiments were performed in 0.5 mol L^{-1} ethanol + 0.1 mol L^{-1} $HClO_4$ solution. The chronoamperometric experiments were performed at 0.5 V (*vs.* RHE) for 2 h. Cyclic voltammogram experiments were recorded within the potential region 0.05–1.2 V (*vs.* RHE), in order to avoid activity decay due to Pt mass losses at high electrode potentials.

Additionally, FTIR *in situ* experiments were performed in a Nicolet Nexus 680 spectrometer using a conventional spectroelectrochemical cell. A planar ZnSe window was used in order to achieve frequencies down to 600 cm^{-1}. Initially, the cleanliness of the electrochemical system was checked cycling the Pt modified Au surface in a fresh 0.1 mol L^{-1} $HClO_4$ solution. After that, ethanol was admitted in the cell at controlled potential in the required amount to produce a 0.5 mol L^{-1} ethanol solution. A 50 mV potential step program was applied from 0.05 to 1.2 V while spectra were recorded. The resolution used in all spectroscopic experiments was 8 cm^{-1} and all spectra were taken as the average of 100 interferograms.

Samples used in X-ray photoelectron spectroscopic experiments were prepared using the procedure mentioned earlier and then transferred to the UHV chamber. The pressure during the measurements was always less than 2×10^{-8} mbar. A VSW HA-100 spherical analyzer and unmonochromatized AlK_α radiation ($h\nu$ = 1486.6 eV) was employed. The high-resolution spectra were measured with a constant analyzer pass energy of 44–22 eV, which produce a full width at half-maximum of 1.6 eV for the Au(4f7/2) line. The 4d and 4p lines of Pt and Au were analyzed using a Doniach–Sunjic and mixed (Gaussian-Lorentzian) lineshapes available in the WinSpec fitting software for metal–metal and metal–O contributions, respectively.[10] Prior to fitting, the X-ray satellites and Shirley background were subtracted from the data. O 1s line was deconvoluted using mixed functions in order to separate contributions from different oxygen-containing species.

Results and discussions

Fig. 1A shows the voltammetric profile of a polycrystalline gold electrode in contact with the base electrolyte (black line) and $CuSO_4$ (grey line) solution. As can be seen from Fig. 1B,

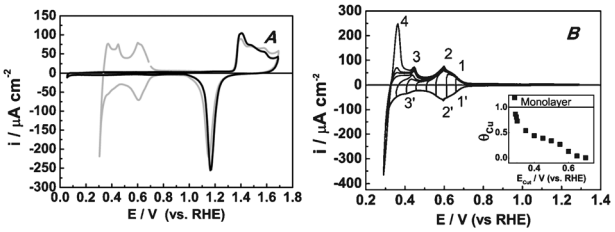

Fig. 1 (A) Cyclic voltammograms for Au in 0.1 mol L^{-1} $HClO_4$ (black line) and 50 mmol L^{-1} $CuSO_4$ + 0.1 mol L^{-1} $HClO_4$ (grey line). (B) Cyclic voltammograms recorded for different potential cuts in 50 mmol L^{-1} $CuSO_4$ + 0.1 mol L^{-1} $HClO_4$. Inset: θ_{Cu} *vs.* E_{cut}, with θ_{Cu} calculated from the cathodic wave. Sweep rate: 50 mV s^{-1}.

the copper monolayer completion occurs at ~0.3 V. The peaks observed in Fig. 1B, as already reported in the literature, can be assigned to different interactions of the Cu ad-atoms with the substrate.[11] According to these authors, peaks 1, 2, 1′ and 2′ can be attributed to a deposit having a strong interaction with the Au substrate. Peak 3′ was associated with copper deposits having $\theta > 1/2$, while peak 3 associated with the dissolution of these deposits. Peak 4 can be related to the dissolution of the Cu deposit resulting from the OPD process below ~0.3 V.

Once the copper monolayer was deposited, the galvanic exchange was allowed to occur in a Pt^{2+} solution, leading to a Pt^{II} deposit, or a Pt^{4+} solution resulting on a Pt^{IV} deposit. Therefore, allowing the deposition of a hypothetical monolayer or half monolayer of Pt, respectively. The voltamperometric profiles of such Pt deposits are shown in Fig. 2.

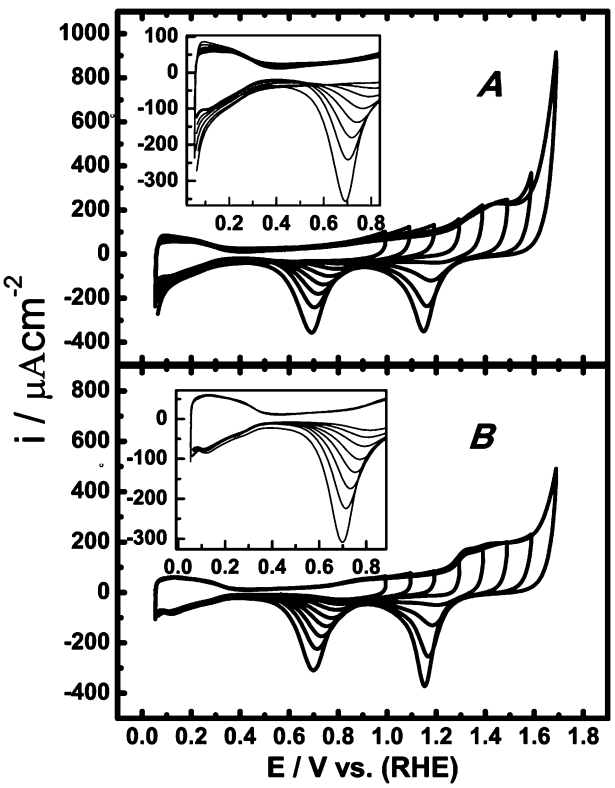

Fig. 2 Cyclic voltammograms for the Pt modified Au electrode in $HClO_4$ 0.1 mol L^{-1}. Sweep rate: 50 mV s^{-1}. (A) Au surface modified with $[PtCl_6]^{2-}$ and (B) with $[PtCl_4]^{2-}$.

3.1 Electrochemical stability of the Pt deposits

As can be seen from Fig. 2 the cyclic voltammograms of the Pt modified Au electrodes seem to result from the superimposition of the cyclic voltammograms for pure Pt and Au. It is possible to notice a hydrogen adsorption/desorption in the potential region at 0.05–0.35 V and the characteristic reduction peaks of Pt and Au oxides at *ca.* 0.7 V and 1.18 V, respectively. Two oxygen adsorption regions can be seen for both Pt deposits, although the Pt^{II} deposit shows a more defined profile for platinum oxide formation, a result that is compatible with the higher Pt content. The first plateau observed in the potential region at 0.7–1.2 V can be attributed to the oxygen adsorption on the platinum active sites. From 1.2 to 1.6 V the oxidation of the Au surface takes place on both samples. A sudden increase of current density is observed beyond 1.6 V that can be assigned to oxygen evolution reaction. The voltammetric profiles obtained for both deposits are in accordance with the data already reported in the literature for Pt–Au alloys,[12,13] Pt overlayers on the Au substrate[14–17] and Pt–Au nanoparticles.[4,18,19]

According to the Pt–Au phase diagram,[20] for Au percentages higher than 20% two phases coexist at room temperature, known as Au- and Pt-rich alloys or α_1 and α_2, respectively. These two phases have, according to Breiter,[21,22] the same hydrogen/oxygen electrosorption properties as the pure constituents of the alloy. Below 20% of Au, a single alloyed phase exists at room temperature known as α-phase with a FCC crystalline structure.[12] However, these data are related to bulk alloy formation and the surface behavior of these alloys can be quite difficult to evaluate in an electrochemical environment. For instance, according to Woods,[13] when Pt–Au alloys are submitted to a potential cycling process the surface composition of the electrode may change, giving rise to a phase segregation into $\alpha_1 + \alpha_2$ at the surface, whatever the bulk composition of the alloy. As a consequence, the voltammetric profiles of the deposits should mimic those for pure platinum and gold, provided that the α_1 and α_2 phases have the same electrochemical properties of their corresponding pure constituents.

As can be seen from Fig. 2, the stability of the Pt deposits towards what we call anodic cycling is quite different, since the hydrogen adsorption/desorption region does not stabilize in the case of the Pt^{IV} deposit. The hydrogen adsorption/desorption region of Pt^{II} remains almost unchanged relative to anodic potential variation up to 1.4 V (E_{cut}). For higher potential values, the hydrogen region profile changes probably due to restructuring of the Pt deposits. Since each voltammetric curve is normalized by the electroactive area, the differences observed in the hydrogen adsorption/desorption region among all voltammograms are no longer attributable to changes in the active surface area. In order to compare the stability of both deposits, the area under the normalized hydrogen desorption region was calculated for each voltammogram and for each E_{cut}. Standard deviation of the values thus obtained revealed that values calculated for the Pt^{IV} deposit vary 2.5 times more than those obtained for the Pt^{II} deposit. This behaviour can be attributed to differences in the stability of each deposit. The variations observed can be associated either with Pt mass losses, as a consequence of a dissolution process taking place throughout the cycling procedure,[23] or to the migration of Pt atoms to the Au crystalline phase.[24]

As stated by Nørskov *et al.*,[25] the deposition of small amounts of Pt on a Au(111) surface induces the formation of a substitutional alloy in the most top layers of the gold crystal. Using scanning tunneling microscopy they suggested that at $\theta_{Pt} < 3\%$ Pt substitution of Au surface atoms occurs leading to the formation of a surface alloy and two dimensional gold islands. As far as the Pt content increases these islands begin to develop with mixed composition of Pt and Au and finally the nucleation of a second layer made of clean platinum islands takes place. They also mentioned that a randomly mixed layer is unstable and that there exists a driving force that will eventually allow the diffusion of Pt atoms into the gold crystal structure, away from the surface. However, this process is kinetically delayed at room temperature and hence a partial capping of Pt by Au atoms occurs at room temperature. Taking into account these results, changes in the voltammetric profiles due to the cycling procedure employed in this work to assess the stability of the deposits could be attributed to the loss of Pt inside the Au crystal structure. The reason why the Pt^{II} deposit shows a higher stability may lie with the fact that higher platinum loading results in lower density of unsaturatively coordinated Pt atoms, a higher number of bound neighbors, more Pt–Pt bonding and lower surface energy excess, thus stabilizing the platinum layer.

Despite the results reported by Rincón *et al.*[14] in which no monolayer (ML) pinholes were observed for $\theta_{Pt} = 1$–30 ML for the same deposition procedure, our Pt^{II} deposits evidence an uncovered Au surface in contact with the electrolytic solution as evidenced by the occurrence of the peak at *ca.* 1.18 V in Fig. 2. Electro-active surface areas were calculated for both Pt deposits (from a hydrogen desorption peak) and the unmodified Au electrode (from the oxide electro-reduction peak). When these values are compared according to Scheijen *et al.*,[16] we find that the surface area for Pt deposits corresponds to 13% (Pt^{IV}) and 32% (Pt^{II}) of the Au surface area. The fact that these values are well below those expected for the ideal layer deposition (50 and 100% respectively) indicates the formation of Pt islands or clusters on the Au surface.

Fig. 3 shows the voltammetric profile of both deposits and that of polycrystalline Pt. As can be seen, when comparing the

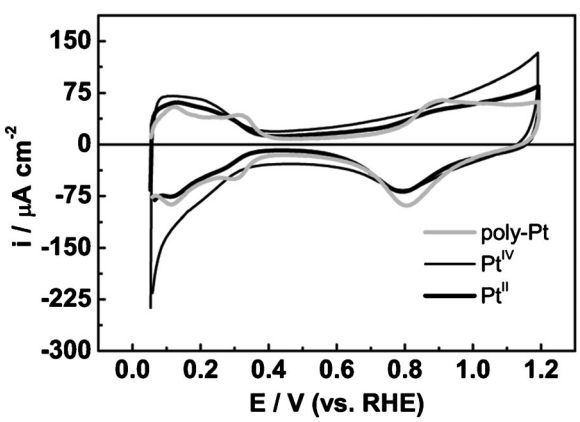

Fig. 3 Cyclic voltammograms for the Pt modified Au electrodes and polycrystalline Pt in $HClO_4$ 0.1 mol L^{-1}. Sweep rate: 50 mV s^{-1}.

reduction potential of PtO_x species for both Pt deposits with that of polycrystalline Pt under the same experimental conditions (*ca.* 0.8 V *vs.* RHE), a small shift in E_{peak} toward lower values is observed for Pt^{IV} and Pt^{II} material. The shifting observed in E_{peak} has already been noticed for other Pt-based alloys by Fernandes *et al.*[26] and was ascribed to a variation in the strength of adsorption of oxygenated species on Pt active sites, owing to the modification of the electronic structure of Pt. In this sense, the gold substrate seems to modify the electronic properties of Pt, leading to an alteration of the adsorptive properties of this phase. This issue will be discussed in more detail in Sections 3.3 and 3.4.

3.2 CO and ethanol electro-oxidation

CO oxidation. TPD experiments performed by Nørskov and co-workers[25] have shown that for $\theta_{Pt} < 0.5$ the temperature of CO maximum desorption (T_{max}) is below the value expected for Pt(111) (418 K). For $0.5 < \theta_{Pt} < 1.3$, the T_{max} increases beyond the value reported for Pt(111) as the Pt content increases. Finally, at $\theta_{Pt} > 1.5$ the value begins to fall approaching that for Pt(111). This behavior can be understood in terms of the structure changes experienced by the deposit due to θ variations. The authors established three types of behaviors: (i) CO adsorption on isolated Pt atoms at low Pt coverage, leading to low adsorption energies of CO and hence temperatures of maximum desorption below that expected for Pt(111); (ii) CO adsorbed on the mixed Au–Pt islands at intermediate Pt coverage values, leading to higher temperatures of maximum desorption than for Pt(111); (iii) for pure Pt islands ($\theta_{Pt} > 1.5$) the CO temperature approaches that of clean Pt(111).

The ideal platinum coverages used in this paper were 0.5 and 1.0. According to Nørskov's results previously mentioned, the temperatures of maximum desorption of CO for these coverage values are higher than for pure Pt. This implies that CO is more strongly bound to Pt in the deposits than in pure platinum. This fact should be reflected in the onset potential value for CO electro-oxidation experiments. If so, the order for the onset potential values should be as follows: poly-Pt < Pt^{IV} < Pt^{II}. However, the substrate used in Nørskov's work was Au(111) and a different tendency could be found when, as in the present report, a polycrystalline gold surface is employed.

With the aim of examining the oxidation of a pre-adsorbed monolayer of CO on the Pt deposits, the O–C–O stretching band of CO_2 was monitored using FTIR *in situ* spectroscopy. In Fig. 4 the integrated CO_2 FTIR band is plotted against potential. This experiment allows us to establish the potential at which CO oxidation begins. As can be seen, the CO monolayer oxidation on the poly-Pt surface starts at 250 mV, while for the Pt deposits the values observed are 400 and 500 mV for Pt^{II} and Pt^{IV} deposits, respectively. This is in accordance with the results reported by Rincón[14] and Du[17] *et al.*, where the onset potential values diminish as the platinum coverage increases. However, comparing our results with the potential onset obtained by Rincón *et al.* for $\theta_{Pt} = 1$, a difference of −100 mV is observed, a fact that could be related with the potential applied for monolayer adsorption (0.05 V in our experiments and 0.09 V in Rincón's work). Any contribution from adsorbed CO on Au is discarded since, as already reported by Mrozek *et al.*,[15] CO adsorption on gold is weak and can be prevented by N_2 purging after CO bubbling.

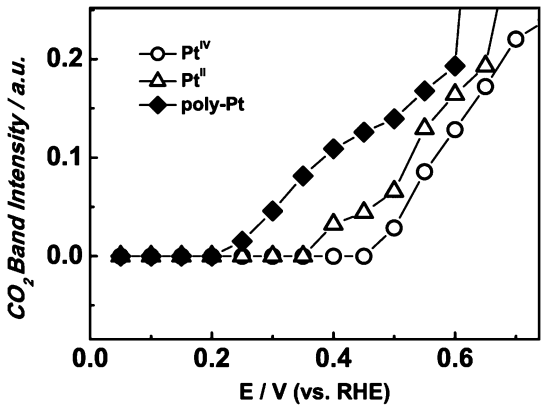

Fig. 4 Amounts (Q) for CO_2 for Pt deposits and polycrystalline Pt formed along the potential excursion in the CO stripping experiment.

Ethanol oxidation. The ethanol electrooxidation voltammograms obtained for both Pt deposits as well as for polycrystalline Pt (poly-Pt) are shown in Fig. 5A. Chronoamperometric results are shown in Fig. 5B. As can be seen from Fig. 5A, current density values follow the order Pt^{IV} > Pt^{II} > poly-Pt, as already reported in the literature for methanol oxidation.[7,16,17,27]

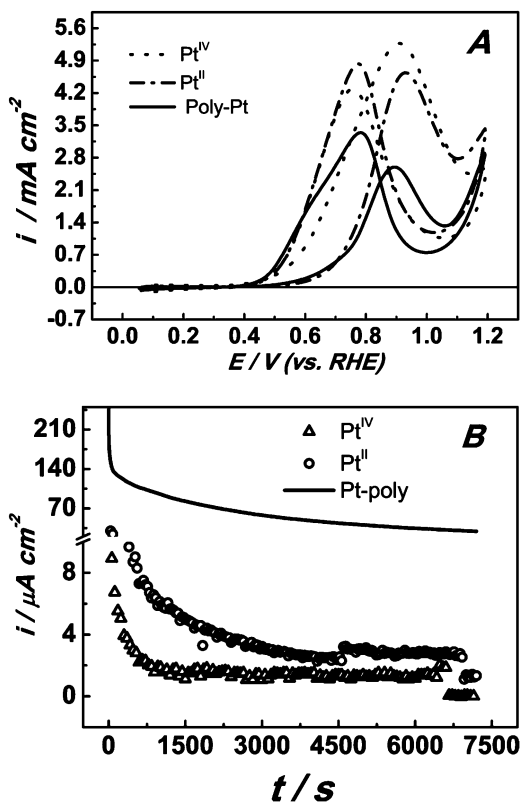

Fig. 5 Ethanol electrooxidation experiments for bare Pt and Pt modified Au substrate in 0.5 mol L^{-1} ethanol + 0.1 mol L^{-1} $HClO_4$, recorded at 50 mV s^{-1}. (A) Cyclic voltammogram for ethanol oxidation and (B) chronoamperometric curves taken at 0.5 V for 2 h.

The onset potential of the electro-oxidation reaction follows the same order, with approximately −200 mV shift for Pt^{IV} with respect to poly-Pt. Additionally, the reactivation peak potential for both platinum deposits is shifted by +45 mV with respect to poly-Pt. Despite these voltammetric features, both deposits appear to suffer a faster deactivation when compared with the polycrystalline electrode under potentiostatic conditions (see Fig. 5B for $t < 700$ s). At $t > 3700$ s the differences in activity are minimized, even though Pt^{II} still presents a higher activity within the experimental error.

The differences in voltammetric profiles for these materials in the oxygen reduction reaction (RRO) and/or methanol and formic acid oxidation have been explained in terms of an improvement in the platinum utilization as a consequence of better dispersion of the platinum phase on the supporting material.[7,28] However, these trends can be understood in terms of the product yield, since current density obtained from the electrochemical system is a function of product distribution. Products formed along the potential excursion program were monitored using *in situ* FTIR measurements. In Fig. 6 spectral series are shown in order to illustrate the bands observed during the experiment. The series shown belong to the Pt^{II} deposit, but those for Pt^{IV} and poly-Pt show similar spectral features. The band assignments were made according to the data presented in the literature for polycrystalline and/or single crystalline platinum electrodes[29–32] (see Table 1).

In order to compare the product yields of the ethanol oxidation over the Pt deposits, CO_2 (2343 cm^{-1}), acetic acid (1280 cm^{-1}) and acetaldehyde (932 cm^{-1}) bands were integrated and the amounts (Q) of product formed during the reaction were calculated following the method proposed by Gao *et al.*[33] and used by Weaver and Iwasita *et al.*[31,32] The values obtained and their dependence on potential can be seen in Fig. 7. From Fig. 7A, we conclude that Pt^{IV} has a higher production of CO_2 when compared to Pt^{II} and poly-Pt. Additionally the acetaldehyde production (Fig. 7C) is retarded to potentials up to 700–750 mV, *i.e.* 350 mV higher than in the case of poly-Pt. However, the potential onset for the production of acetic acid (see Fig. 7B) follows the order: $Pt^{IV} > Pt^{II} >$ poly-Pt.

Table 1 Band frequencies for identified species

ν/cm^{-1}	Assignment
2343	CO_2 (asym., str.)
1717	–CO str. (carbonyl group)
1280	Acetic acid (–COOH group)
1111	Perchlorate ions
1045	Ethanol (C–C–O str.)
932	Acetaldehyde (–C–C–O, asym. str.)

Based on the experimental results and considering the schematic representation of the parallel pathways for the ethanol oxidation mechanism proposed by Camara and Iwasita,[31] the total faradaic current density can be considered as a sum of the individual contribution of each parallel pathway, at each electrode potential value. Thus,

$$i_{total} = i_{CO_2} + i_{Acetaldehyde} + i_{Acetic\ acid} \quad (1)$$

where i_{CO_2}, $i_{Acetaldehyde}$ and $i_{Acetic\ acid}$ represent the individual contribution of all the CO_2, acetaldehyde and acetic acid production paths. Taking into account that each path accounts for a certain amount of electrons for each ethanol molecule and that current density is directly proportional to the number of electrons involved in the path, each path will contribute to the total current density in different proportions. For instance, the CO_2 path is characterized by the transference of 12 electrons for each ethanol molecule, while acetaldehyde and acetic acid paths involve 2 and 4 electrons per ethanol molecule, respectively. In the case of Pt^{IV}, CO_2 and acetic acid production is enhanced; hence, an increment in current density is expected with respect to polycrystalline platinum, since their contribution to the total faradaic current density increases. In Pt^{II}, CO_2 production remains almost the same as in polycrystalline Pt, although acetic acid production is enhanced. In this sense, an increment of current density values is also expected. This would explain why the current densities obtained for Pt^{II} and Pt^{IV} in cyclic voltammograms are higher than that obtained for poly-Pt.

The fact that the acetaldehyde detection is only possible for potentials beyond 0.7 V does not necessarily imply that its production begins at 0.70 V. Due to the fact that acetaldehyde

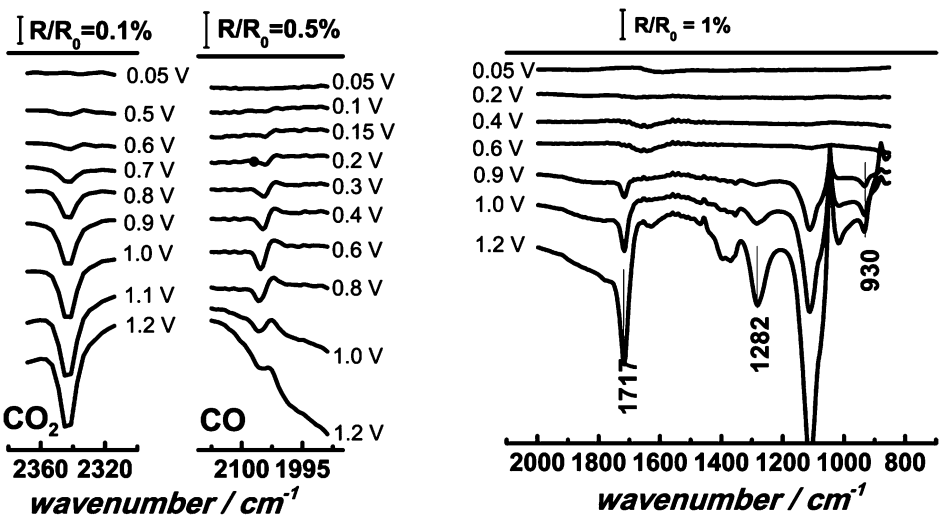

Fig. 6 FTIR spectra for the ethanol electro-oxidation of a Pt^{II} modified Au surface.

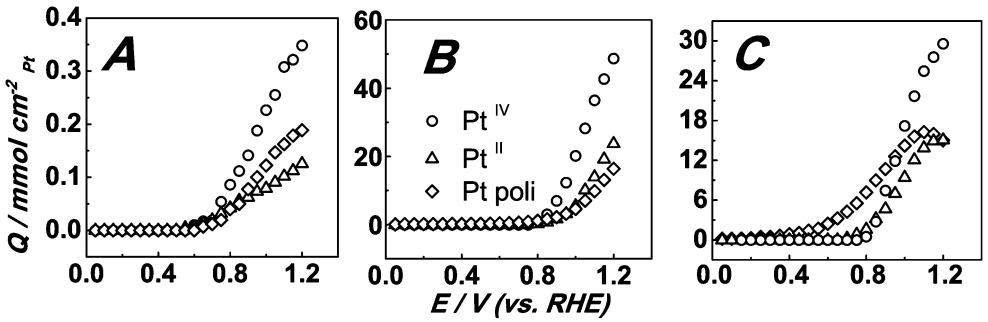

Fig. 7 Amounts (Q) for CO_2 (A), acetic acid (B) and acetaldehyde (C) formed on Pt deposits and polycrystalline Pt as a function of electrode potential.

can suffer either the oxidation to acetic acid or to CO_2, it could be possible that the path acetaldehyde → CO_2 is being favored at potential below 0.7 V, contributing in this way to the CO_2 band intensity increment and maintaining the acetaldehyde concentration below the detection limit. Once acetaldehyde begins to accumulate in the interface, its oxidation to acetic acid begins to play an important role and the further accumulation of this species in the thin layer cavity gives rise to the band at *ca.* 1280 cm^{-1} (also at potential beyond 0.7 V). The lack or even the sluggishness of the acetaldehyde → CO_2 path in polycrystalline platinum would be the explanation for the fact that the band at *ca.* 930 cm^{-1} begins to develop earlier (0.4 V).

According to Dumesic and co-workers[34] the transition state for the C–C bond breaking directly from ethanol or from the acetaldehyde precursor over a Pt(111) surface has similar energies (1.5 eV). However, the most stable precursor indicated as responsible for the C–C rupture is the CHCO species. In order to achieve the formation of the C–C breaking precursor the ethanol molecule should undergo successive dehydrogenation steps. These steps could be favored in the Pt–Au alloyed sites, since Au might not be inert, as already pointed out by Bus and Bokhoven.[35] In their publication they have demonstrated using X-ray absorption spectroscopy that hydrogen adsorption can take place on Pt and Au sites on Pt–Au alloys, although adsorption on Au sites is weaker. Additionally, Chandler *et al.*[36] proposed that CO could also be adsorbed onto Au sites besides the usual Pt ones, although with a much weaker character. Bus and Bokhoven[35] also proposed that CO and hydrogen might not adsorb at the same site since their H/M and CO/M ratios (M stands for metal) are quite different.

Taking into account all the ideas exposed in the last paragraphs, we suggest that Pt and Au sites in Pt–Au alloys, despite the fact of having similar adsorptive properties, *i.e.*, both have the ability to adsorb either CO or H at different extensions, they might act in a complementary way adsorbing different intermediary species. Thus, Au sites could assist the Pt sites adsorbing intermediary species and hence, releasing the Pt active sites that otherwise would be blocked by those species. On the other hand, the H_2O activation process could be affected by the electronic and geometric properties of the Pt deposits and consequently the availability of the oxygenated species necessary for further oxidation of some reaction intermediates (CO/CH_x).

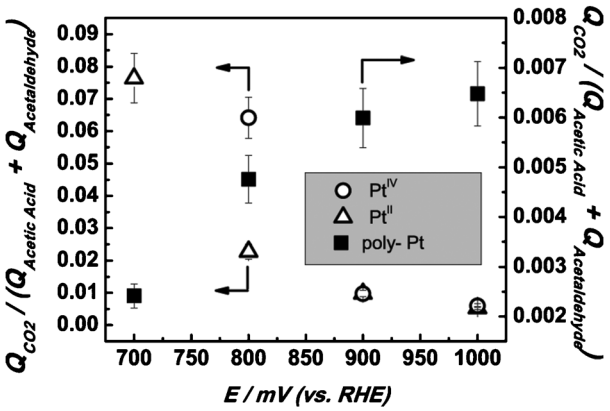

Fig. 8 $Q_{CO_2}/(Q_{\text{Acetic acid}} + Q_{\text{Acetaldehyde}})$ ratios calculated from data in Fig. 7.

With the aim of detecting possible changes in the reaction pathways of the ethanol oxidation mechanism, the $Q_{CO_2}/(Q_{\text{Acetic acid}} + Q_{\text{Acetaldehyde}})$ ratios were calculated for different potentials from data shown in Fig. 7. This ratio can be taken as a measure of the intrinsic ability of the material to cleave the C–C bond since active or geometric area effects are avoided. Nevertheless, it is important to note that the ethanol oxidation reaction mechanism is also potential dependent, as the electronic properties of the material change with potential, which in turn modifies the adsorption strength of the adsorbed intermediates. As shown in Fig. 8, the ratios calculated for both platinum deposits are approximately 10 times higher than the values obtained for poly-Pt. This fact constitutes an additional proof that, in the case of Pt^{II} and Pt^{IV} modified surfaces, the reaction path that corresponds to C–C bond breaking (CO_2 production) is being favoured instead of those involving a lower number of electrons (acetic acid and/or acetaldehyde). Additionally, the potential dependencies are opposite, since for both deposits the ratio values decrease as the potential increases while for poly-Pt the ratio increases as the potential increases.

3.3 XPS characterization

Fig. 9 shows the X-ray photoelectron spectra recorded for the platinum deposits together with the curves obtained in the fitting procedure. Table 2 summarizes the parameters calculated in the fitting procedure. As can be seen from the table, the Pt $4d_{5/2}$ lines are shifted to lower binding energy (BE) values. The same behaviour was observed for the Pt$4p_{3/2}$ line.

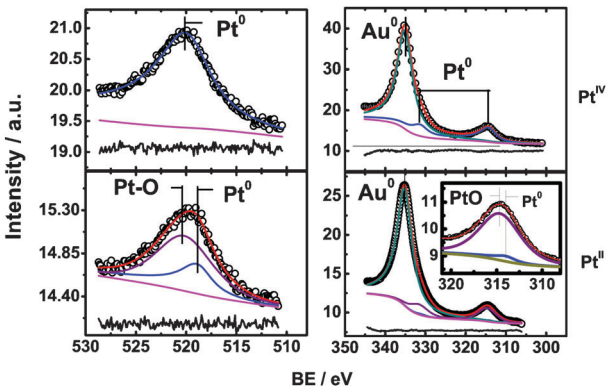

Fig. 9 XPS spectra for platinum deposits showing the contributions considered in the deconvolution procedure. Solid line at the bottom in all figures represents fitting residue.

Table 2 Parameters calculated from the deconvolution procedure used in XPS analysis

Parameter	Pt^{II} deposit	Pt^{IV} Deposit	Reference value
Pt $4d_{5/2}$/Pt–Pt	313.9	314.07	314.4
Pt $4d_{5/2}$/Pt–O	314.7	—	
Pt–O 4d : O 1s ratio	1.14	—	1
Pt : Au ratio ($4p_{3/2}$)	0.5370	0.2788	—

Several groups have reported that a negative shifting in BE values of Au and Pt 4f lines is observed when Pt is alloyed with Au.[10,37,38]

From the XPS experiments we conclude that in the case of the Pt^{II} modified surface (ideal monolayer), two kinds of Pt atoms can be distinguished: (i) those that are alloyed with Au atoms located at the interface between Au and Pt and (ii) those that are at the topmost surface and that are not alloyed with Au and hence oxidize once the sample is exposed to air (see Fig. 8c of ref. 25). This would explain the detection of the Pt–O Gaussian component in the XPS spectra. The (Pt–O)/O ratio calculated using the area values obtained from the fitting and the corresponding cross sections reported by Yeh and Lindau[39] for Pt 4d and O 1s lines are in accordance with that expected (1 : 1), and can be taken as an indicative of the fitting reliability. The likelihood of the fitting can be evaluated by plotting the fitting residues in Fig. 9 below every peak fitting.

However, for the Pt^{IV} sample, no Pt-oxide contribution was observed. Instead, only a metallic Pt contribution was found to occur at 314.04 eV for the $4d_{5/2}$ line. As can be seen from Table 2, the BE values obtained for Pt lines were shifted toward lower values such as in the Pt^{II} sample. These observations could be explained in terms of the morphologies adopted by the deposit at this coverage (see Fig. 8b of ref. 25).

The differences between the two samples analyzed by XPS can be explained as follows. At relatively low θ_{Pt} (*e.g.* 0.5) the Pt atoms displace the topmost Au surface atoms leading to the formation of Au 2D islands and a superficial substitutional alloy. In this case the Pt atoms are incorporated in the Au crystalline structure and the property for oxygen adsorption changes from that of pure Pt. However, as θ_{Pt} increases Pt atoms begin to deposit over the bidimensional islands previously formed by Au atoms. These Pt atoms would be able to oxidize under certain experimental conditions giving rise to the Pt–O contribution found. In this fashion, Pt migration into gold's crystalline structure seems to act as a protection preventing the oxidation of the deposit.

On the other hand, as stated earlier in section 3.2.2, the deposit structure can influence its own property for water activation or even adsorption of O–containing species. For instance, the bidimensional Au islands formed along the deposition process should present differentiated adsorption properties compared to bare gold, and some properties that are not present in smooth Au surfaces might emerge on this surface 2D arrangements. This variations would be mirrored on the catalytic response of the material and confirm the observation made by other authors about the lack of inertness.

3.4 General considerations

Considering the results shown in previous sections it remains clear that both Pt deposits deactivate faster during ethanol oxidation reaction when compared to polycrystalline platinum. Also, two phases were identified through XPS measurements, being Pt atoms alloyed with the topmost Au atom layer of the substrate and a phase that resembling pure Pt. The relative proportion of these two phases seems to depend on Pt coverage, being the alloyed phase the one that prevails at the low Pt content. As a consequence of alloy formation, the electronic structure of Pt change and an upward shift in the d states are noticed. According to the d-band centre model introduced by Nørskov and coworkers,[40,41] the higher the d-band centre in the energy scale, the stronger is the adsorbate-metal interaction, since new antibondig states above the Fermi level are formed as the d-band centre is shifted upwards.

Two different conditions were used in the present paper: potentiodynamic and potentiostatic. Results obtained under each condition seem to disagree, but they can actually be explained by the following argument. Under potentiodynamic conditions, the presence of defects (undercoordinated atoms generated throughout the substitution process of Au surface atoms by Pt) becomes important and C–C bond in each ethanol molecule breaks easier than in a surface containing a lower concentration of defect. Thus, CO residues resulting from bond breaking are progressively oxidized as electrode potential increases.

On the other hand, when potentiostatic condition is applied, *e.g.* in chronoamperometric experiments, CO molecules begin to accumulate in the active sites of the Pt–Au surface faster than in a pure Pt surfaces, since CO-M adsorption in Pt–Au surface is stronger than in bare Pt. In this sense, the electronic effect turns out to be important in this situation, leading to a poisoning of the catalytically active phase. The reason why Pt^{IV} deposit deactivates faster than Pt^{II} deposit is related to the fact that, some pure Pt active centres remain unalloyed in the last one, and hence catalytic behaviour should be similar to pure Pt.

Conclusions

Platinum deposits turned out to be stable for potentials of up to 1.2 V (*vs.* RHE), although Pt^{II} showed a higher stability compared to the Pt^{IV} deposit. This result was explained in terms of the reactivity of the clusters formed on the substrate

surface. Pt migration or dissolution processes were pointed out as possible sources of instability due to anodic cycling.

On the other hand, both Pt deposits presented the ability to break the C–C bond present in the ethanol molecule as demonstrated by *in situ* FTIR results; however, a faster deactivation is observed on Pt deposits when subjected to potentiostatic conditions as confirmed by chronoamperometric results shown. The differences in the catalytic response were explained in terms of the structures adopted by the Pt layer on the gold substrate. As demonstrated by XPS measurements, the lower Pt coverage used in this paper presented a higher alloying degree with the topmost Au atom layer, leading to the formation of Au islands, which were intended to have a differentiated surface chemistry compared to bare Au.

Acknowledgements

Authors thank *Conselho Nacional de Pesquisa (CNPq) and Fundação de Amparo à Pesquisa do Estado de São Paulo (FAPESP)* for the financial support. MJP thanks CNPq for the fellowship granted (Proc. 142507/2007-5).

References

1 S. R. Brankovic, J. X. Wang and R. R. Adzic, *J. Serb. Chem. Soc.*, 2001, **66**, 887–898.
2 H. Inoue, S. R. Brankovic, J. X. Wang and R. R. Adzic, *Electrochim. Acta*, 2002, **47**, 3777–3785.
3 R. R. Adzic, *Electrochim. Acta*, 2007, **52**, 7.
4 J. Luo, P. N. Njoki, Y. Lin, D. Mott, L. Y. Wang and C. J. Zhong, *Langmuir*, 2006, **22**, 2892–2898.
5 J. H. Huang, Q. J. Xie, Y. M. Tan, Y. C. Fu, Z. H. Su, Y. Huang and S. Z. Yao, *Mater. Chem. Phys.*, 2009, **118**, 371–378.
6 S. Y. Wang, N. Kristian, S. P. Jiang and X. Wang, *Nanotechnology*, 2009, **20**, 1–9.
7 N. Kristian and X. Wang, *Electrochem. Commun.*, 2008, **10**, 12–15.
8 M. D. Obradovic, A. V. Tripkovic and S. L. Gojkovic, *Electrochim. Acta*, 2009, **55**, 204–209.
9 X. Ge, R. Wang, S. Cui, F. Tian, L. Xu and Y. Ding, *Electrochem. Commun.*, 2008, **10**, 1494–1497.
10 S. E. Hörnström, L. Johansson, A. Flodström, R. Nyholm and J. Schmidt-May, *Surf. Sci.*, 1985, **160**, 561–570.
11 A. J. Motheo, E. R. Gonzalez, A. Rakotondrainibe, J.-M. Léger, B. Beden and C. Lamy, *J. Braz. Chem. Soc.*, 1996, **7**, 1–6.
12 B. Brown, S. D. Wolter, B. R. Stoner and J. T. Glass, *J. Electrochem. Soc.*, 2008, **155**, B852–B859.
13 R. Woods, *Electrochim. Acta*, 1971, **16**, 655–659.
14 A. Rincón, M. C. Perez and C. Gutierrez, *Electrochim. Acta*, 2010, **55**, 3152–3156.
15 M. F. Mrozek, Y. Xie and M. J. Weaver, *Anal. Chem.*, 2001, **73**, 5953–5960.
16 F. J. E. Scheijen, G. L. Beltramo, S. Hoeppener, T. H. M. Housmans and M. T. M. Koper, *J. Solid State Electrochem.*, 2008, **12**, 483–495.
17 B. Du and Tong, *J. Phys. Chem. B*, 2005, **109**, 17775–17780.
18 M. M. Maye, N. N. Kariuki, J. Luo, L. Han, P. Njoki, L. Wang, Y. Lin, H. R. Naslund and C.-J. Zhong, *Gold Bull.*, 2004, **37**, 8.
19 J. B. Xu, T. S. Zhao, W. W. Yang and S. Y. Shen, *Int. J. Hydrogen Energy*, 2010, **35**, 8699–8706.
20 G. C. Bond, *Platinum Met. Rev*, 2007, **51**, 6.
21 M. W. Breiter, *J. Phys. Chem.*, 1965, **69**, 901–904.
22 M. W. Breiter, *Trans. Faraday Soc.*, 1965, **61**, 749–754.
23 V. Komanicky, K. C. Chang, N. M. Markovic, H. You, X. Wang and D. Myers, *J. Electrochem. Soc.*, 2006, **153**, B446–B451.
24 E. Rach and J. Heitbaum, *Electrochim. Acta*, 1987, **32**, 1173–1180.
25 M. Ø. Pedersen, S. Helveg, A. Ruban, I. Stensgaard, E. Lægsgaard, J. K. Nørskov and F. Besenbacher, *Surf. Sci.*, 1999, **426**, 395–409.
26 A. C. Fernandes, V. A. Paganin and E. A. Ticianelli, *J. Electroanal. Chem.*, 2010, **648**, 156–162.
27 L. Yang, J. Chen, X. Zhong, K. Cui, Y. Xu and Y. Kuang, *Colloids Surf., A*, 2007, **295**, 21–26.
28 D. Zhao and B. Q. Xu, *Phys. Chem. Chem. Phys.*, 2006, **8**, 5106–5114.
29 T. Iwasita and E. Pastor, *Electrochim. Acta*, 1994, **39**, 531–537.
30 X. H. Xia, H. D. Liess and T. Iwasita, *J. Electroanal. Chem.*, 1997, **437**, 233–240.
31 G. A. Camara and T. Iwasita, *J. Electroanal. Chem.*, 2005, **578**, 315–321.
32 L. W. H. Leung, S. C. Chang and M. J. Weaver, *J. Electroanal. Chem.*, 1989, **266**, 317–336.
33 P. Gao, S.-C. Chang, Z. Zhou and M. J. Weaver, *J. Electroanal. Chem.*, 1989, **272**, 161–178.
34 R. Alcala, M. Mavrikakis and J. A. Dumesic, *J. Catal.*, 2003, **218**, 178–190.
35 E. Bus and J. A. van Bokhoven, *Phys. Chem. Chem. Phys.*, 2007, **9**, 2894–2902.
36 B. D. Chandler, A. B. Schabel, C. F. Blanford and L. H. Pignolet, *J. Catal.*, 1999, **187**, 367–384.
37 N. J. Shevchik, *Phys. Rev. Lett.*, 1974, **33**, 1336.
38 Z. Bastl and S. Pick, *Surf. Sci.*, 2004, **566–568**, 832–836.
39 J. J. Yeh and I. Lindau, *At. Data Nucl. Data Tables*, 1985, **32**, 1–155.
40 B. Hammer and J. K. Nørskov, *Adv. Catal.*, 2000, **45**, 71–129.
41 J. Greeley, J. K. Nørskov and M. Mavrikakis, *Annu. Rev. Phys. Chem.*, 2002, **53**, 319–348.

